Research Article | Vol. 17, No. 4 / 1 Apr 2026 / *Biomedical Optics Express* 2148

Biomedical Optics EXPRESS

Racetrack ring resonator-assisted MZI-based integrated optical biosensor with buffer layers for measuring blood glucose level

KAMAKSHI MANCHIKALAPATI,[1,*] GOPALKRISHNA HEGDE,[2] AND SRINIVAS. TALABATTULA[1]

[1] *Dept of ECE, Indian Institute of Science, Bengaluru, 560012, India*
[2] *Dept of Aerospace Engineering, Indian Institute of Science, Bengaluru, 560012, India*
[*] *kamakshim@iisc.ac.in*

Abstract: In this study, we present a two-racetrack ring assisted Mach-Zehnder interferometer (RRAMZI) configuration, specifically engineered for glucose detection. RRAMZI chose to combine the property of high sensitivity of the racetrack ring resonator (RRR) with the property of high accuracy due to the reference arm of the Mach-Zehnder Interferometer(MZI) for achieving high sensitivity with high accuracy. To enhance biosensor performance, intermediate buffer layers were introduced between the core and substrate layers. Depending on the material chosen for the buffer layer, it offers the advantage of enhancing the resonant and penetration depths. In this paper, two different configurations of RAMZI with two different buffer materials are presented. The two materials of the buffer layer are silicon nitride (Si_3N_4) and fluorinated silicon dioxide ($FSiO_2$). The first Si3N4 buffer layer is strategically introduced between the silicon dioxide (SiO_2) substrate and the silicon (Si) core. The inclusion of the Si_3N_4 layer directly contributes to an increase in resonant depth, which eventually enhances the quality factor to 1.435×10^3. In the second architecture, the $FSiO_2$ layer is introduced between SiO_2 and Si. It enhances penetration depth, which in turn increases the sensitivity of RRAMZI to 400 nm/ RIU. The system is analytically modeled using the signal-flow graph (SFG) method.

1. Introduction

In recent years, the number of diabetic patients has enormously increased. Diabetes is a condition in which the blood glucose level shoots up. Diabetes can lead to several health complications including Cardiovascular, Nervous, Eye etc. It is necessary to monitor glucose level in blood regularly. Due to this the demand for diagnostics devices increases. Photonic Integrated biosensors are a lab-on-a-chip device used for detecting the concentration of blood glucose. It offers the advantage of realizing biosensor at micrometer dimensions with high Sensitivity [1–3].

Common integrated optical devices include the Mach-Zehnder Interferometer (MZI), Ring Resonator (RR), Directional Coupler (DC), and Race- track Ring Resonator (RRR). MZI-based biosensors are advantageous due to the inclusion of a reference arm, which enhances detection accuracy. [4–10]. A silicon microring resonator based on thin-film silicon nitride (Si3N4) waveguides was designed and fabricated for biosensing applications. Fabrication was performed on a silicon nitride wafer with a 250 nm top layer over a 3 μm buried oxide using electron-beam lithography and inductively coupled plasma (ICP) etching. The microring had a radius of 50μm. Bulk refractive index sensing was used, with sodium chloride solutions of different concentrations resulting in spectral shifts. The device exhibited a sensitivity of 384.58 nm/RIU and a limit of detection (LOD) of 4.68×10^{-4} RIU. [11].

Racetrack ring is similar to a ring but has an additional straight waveguide between rings by making more coupled region This work [12] presents an SOI racetrack ring resonator(RRR) refractive-index sensor for the C-band (1500–1600 nm), operating in the TE0 mode. The

#589260 https://doi.org/10.1364/BOE.589260
Journal © 2026 Received 2 Jan 2026; revised 17 Mar 2026; accepted 19 Mar 2026; published 31 Mar 2026

Biomedical Optics EXPRESS

architecture combines two straight-rib bus waveguides with a central circular ring and elongated straight sections, allowing the authors to tune the coupling independently of the bend radius—core-to-racetrack practice. Reported performance metrics are S = 102 nm/RIU, and FOM = 201 RIU. Khozeymeh and Razaghi [13] analyze SiON racetrack resonators with a bent part coupled to a bus waveguide The study engineer via geometry and monitor how local cladding overlap in the bend can tax Qi and influence the intrinsic limit of detection (ILOD). The methodology is uniquely valuable when pulley/bent couplers are necessary. It is also required when footprint constraints prevent the use of long straight couplers. It resolves the trade-off between placement, dispersion, and biosensing figures of merit. Butt et al. [14] report a SiN ring resonator sensor operating at 1543.8 nm. The analytes used are certified Cargille index liquids. The study combines 2D-FEM with experiment and simulated bulk wavelength sensitivity =110 nm/RIU and measured =112.5 nm/RIU.

To address this, RRs are coupled with MZIs to expand the interaction area with the analyte, while still retaining the benefit of a reference arm [8,9], with device dimensions reduced to the micrometer scale. By cascading these components, performance improvements can be achieved in terms of sensitivity(S), figure of merit(FOM), and the quality factor(Q) [14,15,16,17,18,19,27].

Enhancing the resonant depth and penetration depth in Racetrack Ring Resonators (RRRs) is crucial for advancing integrated biosensing platforms, particularly in applications requiring high spectral resolution and sensitivity, such as blood glucose monitoring. This study presents a Racetrack Ring Assisted Mach-Zehnder Integrated (RRAMZI) configuration, engineered explicitly for glucose detection where the RRR is coupled to the sensing arm of the MZI with a buffer layer. The material of the buffer depends upon the requirement, like whether we require a high resonant depth or high penetration depth.

To enhance resonant depth, a silicon nitride (Si_3N_4) buffer layer is strategically introduced between the silicon dioxide (SiO_2) substrate and the silicon (Si) core. This significantly enhances optical mode confinement, suppresses substrate leakage, and improves phase matching, thereby increasing coupling efficiency between the MZI and RRR. Including the Si_3N_4 layer, which directly contributes to increased resonant depth, quality factor, and sensing contrast. To enhance penetration depth a flourinated silicon dioxide ($FSiO_2$) buffer layer is introduced between SiO_2 and Si. This enhances the evanescent field by reducing the mode confinement. This enhancement in penetration depth, in turn increases sensitivity. A simple buffer layer engineering can enhance parameters like resonant depth and penetration depth. The system is analytically modelled using the Signal-Flow Graph (SFG) method.

RRs are coupled with MZIs to expand the interaction area with the analyte, while still retaining the benefit of a reference arm, with device dimensions reduced to the micrometer scale. By cascading these components, performance improvements can be achieved in terms of sensitivity (S), figure of merit (FOM), and quality factor (Q) [19,20].

2. Proposed structure

The proposed device configuration of two is shown in Fig. 1. The bottom layer of the device is the substrate, made of silicon dioxide, with a width of 30 μm and a thickness of 1.71 μm. The next layer is buffer layer. In one configuration silicon nitride buffer layer is deposited above the substrate. This layer has a width of 30 μm and a thickness of 0.10 μm. In other configuration $FSiO_2$ buffer layer is deposited above Substrate. The layer above the buffer layer is silicon, which acts as the core for guiding light. The dimensions of the core layer are same for both configurations. This silicon layer is structured to form the MZI and the RRR. The MZI consists of a Y-splitter, a Y-combiner, and two waveguides. One of the waveguides is connected to the RRR and serves as the sensing arm, while the other functions as the reference arm. The gap between the two arms of the interferometer is 6 μm, and the combined length of the Y-splitter

Biomedical Optics EXPRESS

and Y-combiner is 38 μm. An analyte layer with a thickness of 0.48μm (480 nm) is placed above the sensing region. The structure is shown in Fig. 1.

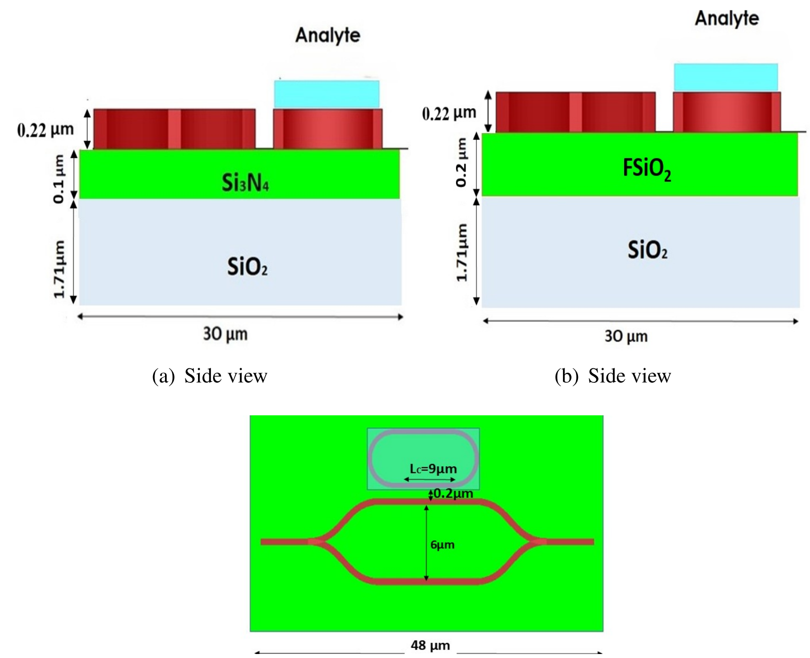

(a) Side view (b) Side view

(c) Top view

Fig. 1. Proposed Structure.

3. Mathematical analysis of output and performance metrics

Here, the SFG method was applied to the Transmission Spectrum, and it was designed using Manson's Gain formula. The advantage of applying it to the proposed design is a reduction in the complexity of calculating the transmission spectrum. Extracted method from the Control Systems book [22].

Mason's Gain Formula: The total transfer function H_{total} of a system is given by:

$$H_{\text{total}} = \frac{\sum_k P_k \Delta_k}{\Delta}, \tag{1}$$

- P_k: Gain of the k-th **forward path** from input to output.

$$\Delta = 1 - \sum(\text{all individual loop gains}) + \sum(\text{gain products of 2 non-touching loops}) \tag{2}$$

- Δ_k: Value of Δ when all loops touching the k-th forward path are removed.

Signal Flow Graph (SFG) for the MZI with RRR E_{in} -Input field, E_t -Field entering the top arm (with the racetrack ring), E_b-Field entering the bottom arm, E_r -circulating field in the ring, E_{out} -output field. H_t -Transfer function of top arm, H_b-Transfer function of bottom arm

1. The splitter splits E_{in}:

$$E_t = \sqrt{0.5}E_{\text{in}}, \quad E_b = \sqrt{0.5}E_{\text{in}} \tag{3}$$

Biomedical Optics EXPRESS

2. The top arm includes the racetrack ring:

$$E_{\text{through}} = tE_t - j\kappa E_r, \quad E_r = \frac{-j\kappa E_t}{1 - te^{-j\phi_r}} \tag{4}$$

Hence, the transfer function of the top arm is:

$$H_t = t + \frac{-\kappa^2 e^{-j\phi_r}}{1 - te^{-j\phi_r}} \tag{5}$$

3. The bottom arm introduces a phase shift:

$$H_b = e^{-j\phi_b} \tag{6}$$

4. The combiner adds the fields from both arms:

$$E_{\text{out}} = H_b E_b + H_t E_t \tag{7}$$

A forward path is any path that directly connects E_{in} to E_{out} without retracing. For this system: Path 1 (via bottom arm), Path 2 (via top arm) and Loop gains

$$P_1 = \sqrt{0.5} H_b \tag{8}$$

$$P_2 = \sqrt{0.5} H_t \tag{9}$$

$$L_1 = te^{-j\phi_r} \tag{10}$$

The total transfer function using the Eqs. (1)-(10) is:

$$H_{\text{total}} = \frac{\sqrt{0.5} H_b \Delta + \sqrt{0.5} H_t \Delta}{\Delta} \tag{11}$$

$$H_{\text{total}} = \sqrt{0.5}(H_b + H_t) \tag{12}$$

The normalized transmission spectrum is:

$$T = \frac{|E_{\text{out}}|^2}{|E_{\text{in}}|^2} = |H_{\text{total}}|^2 . \tag{13}$$

‘

$$T = \frac{1}{2} |H_b + H_t|^2 . \tag{14}$$

$$T = \frac{1}{2} \left| e^{-j\phi_b} + t + \frac{-\kappa^2 e^{-j\phi_r}}{1 - te^{-j\phi_r}} \right|^2 . \tag{15}$$

This is the final **transmission spectrum** using Mason’s Gain Formula.

The derived transmission spectrum reflects the combined effects of interference in the MZI and the resonant properties of the RRR. By varying the input wavelength, the transmission.

4. Performance metrics

4.1. Sensitivity

Sensitivity is defined as the fraction of change in resonant wavelength resulting from a change in effective refractive index due to the application of the analyte. Its units are nm/RIU [21]

$$S = \Delta\lambda_{res}/\Delta n_c \tag{16}$$

where $\Delta\lambda_{res}$ = change in resonant wavelength Δn_c= Change in refractive index of analyte.

Biomedical Optics EXPRESS

4.2. Quality factor

Quality factor is referred to as the fraction of resonating wavelength and the difference of wavelength at Full Width Half Max (FWHM),

$$Q = \lambda_{res}/\Delta\lambda_{FHWM} \tag{17}$$

where λ_{res} = resonating wavelength $\Delta\lambda_{FWHM}$= difference of wavelength at FWHM

4.3. Figure of merit

FOM is referred to as the fraction of Sensitivity and FWHM [10]

$$FOM = S/FHWM \tag{18}$$

Where S = Sensitivity, FWHM =Full Width Half Max

Resonant depth is a crucial metric that affects the sensitivity and Q of the biosensor. It is the difference between the maximum and the minimum of the transmission spectrum.

$$D = T_{max} - T_{min} \tag{19}$$

where T_{max}= Transmission Spectrum Max, T_{min}= Transmission Spectrum Min

5. Optimization of waveguide and selection of buffer material

Initially, the Si waveguide is optimized for single-mode operation by varying the width and thickness of the silicon layer. The optimized dimensions shown in Fig. 2 ensure single-mode operation.

Selection of buffer material is one of the important aspect of proposed biosensor. In this section the material selection is done by plotting the mode field with different refractive index of buffer from 1 to 2. From Fig. 3 it is observed that the mode field is weekly guided as the refractive index is 1.4 indicating more evanescent field resulting more penetration depth. From Fig. 3 it is observed that the field is tightly confined at buffer refractive index 2. This help in increasing resonance depth. Silicon Nitride and Flourinated Silicon dioxide are having refractive index 2 and 1.4.

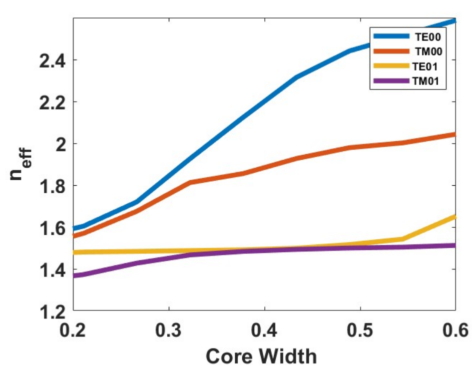

(a)

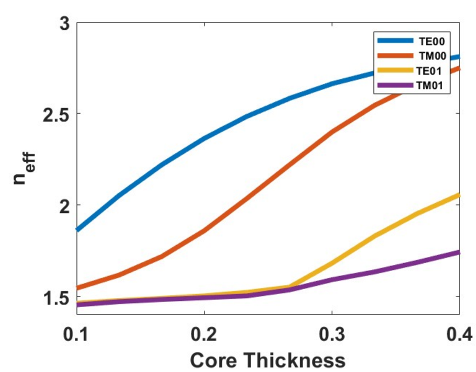

(b)

Fig. 2. variation of n_{eff} with respect to (a) Width (b) Thickness.

Biomedical Optics EXPRESS

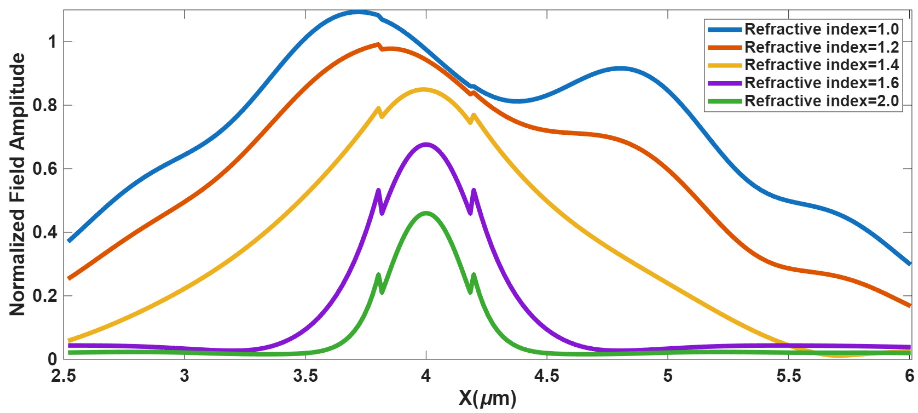

Fig. 3. Modefield Profile Different Refractive Index.

6. Optimization of RRAMZI

Once the waveguide is optimised for single-mode operation and the buffer material is selected, then the RRAMZI parameters like coupling gap, coupling length and ring radius have to be optimised. As the device RRAMZI is coupled configuration the mode field at the coupling region should be plotted to ensure coupling. The mode field coupling of RRAMZI is as shown in Fig. 4.

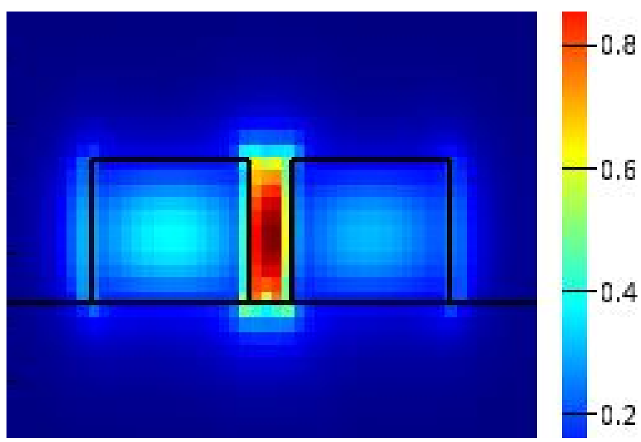

Fig. 4. Coupled region mode field profile.

The coupling gap(G) is the further optimised that ensures maximum coupling between the MZI and the RRR. Stronger coupling leads to improved sensitivity and a higher quality factor. To achieve maximum coupling, the gap between the MZI and RRR is varied from 0.18 μm to 0.22μm. Through this analysis, an optimized G of 0.2 μm is identified and selected for the final biosensor design. Figure 5 shows the transmission spectra for various coupling gaps. At a G of 0.2 μm, the resonant peak appears narrow, indicating a higher quality factor. Therefore, a coupling gap of 0.2 μm is fixed as the optimal value for the proposed structure.

The coupling length (L_C) is a significant parameter that directly affects the sensitivity (S) and quality factor of the biosensor. To achieve optimal performance, the coupling length of the RRR is varied. As shown in Fig. 6, maximum coupling leads to improved sensitivity and an enhanced quality factor. A high Q factor is observed when the coupling length is set to 9 μm.

Biomedical Optics EXPRESS

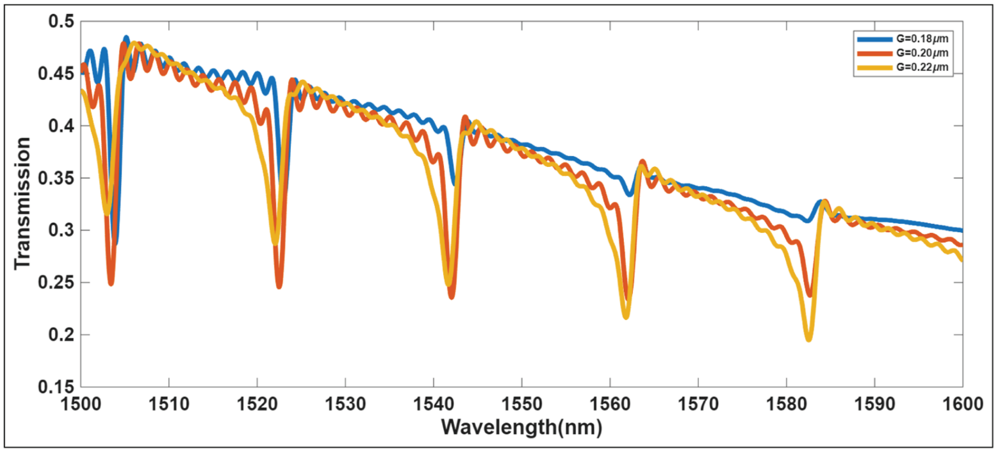

Fig. 5. Transmission Spectrum for different Coupling Gap.

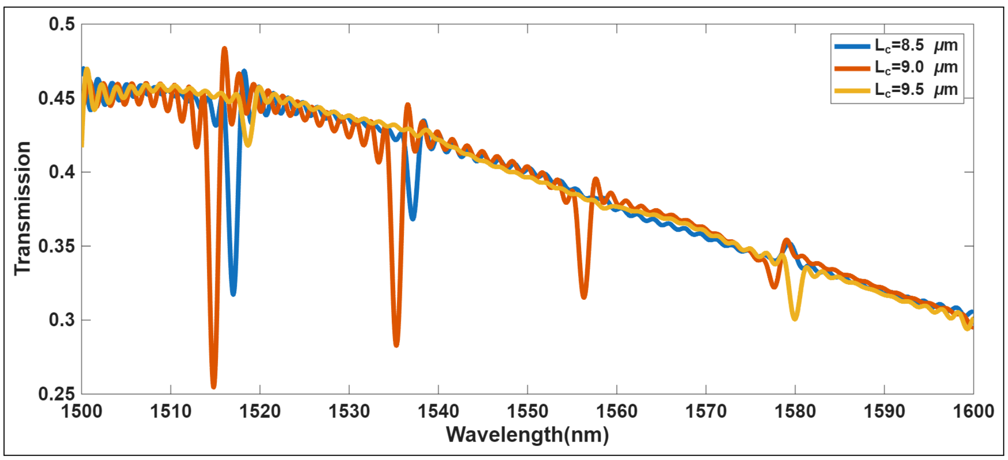

Fig. 6. Transmission Spectrum for Different Coupling Length.

7. RAMZI with Si_3N_4 buffer

7.1. Optimization of buffer thickness

The addition of the Si_3N_4. The layer significantly affects the resonant depth, which in turn influences the sensor's ER [21]. The buffer thickness (T) of the silicon nitride layer is a critical parameter, as it directly impacts the overall performance of the device. Therefore, careful optimization is required. The thickness of this layer was varied from 0.07μm to 0.13μm, and the observed resonant depth. From Fig. 7, a t T=0.1 μm, the resonant depth is high, so it is chosen for designing.

7.2. Comparison with conventional biosensor of the same dimensions

One of the main innovations of this biosensor is the addition of a Si_3N_4 , which allows for greater flexibility in increasing the resonance depth of RRAMZI. This improvement can be evaluated by comparing the transmission at the sensing arm for both configurations, with and without Si_3N_4 layer. Figure 8 presents the transmission results for both setups. The comparison shows that at a

Biomedical Optics EXPRESS

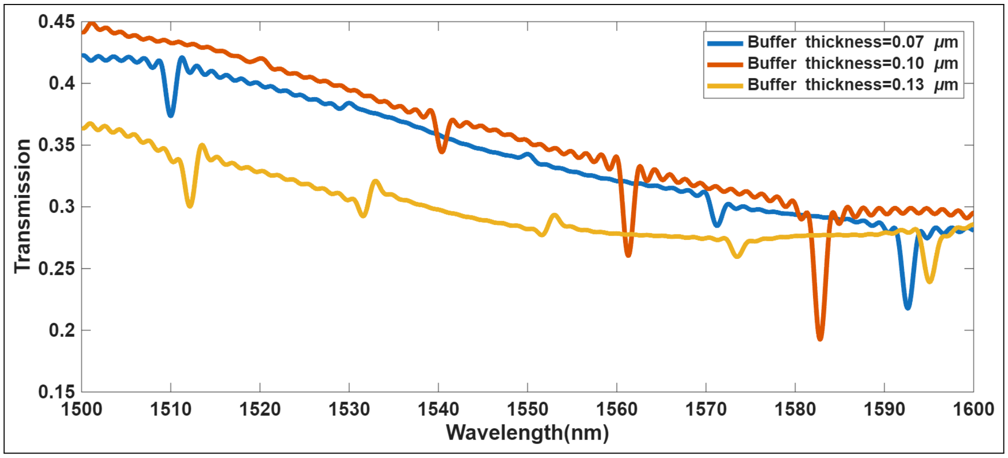

Fig. 7. Transmission spectrum for Different Thickness of Si_3N_4.

100nm gap, the configuration with Si_3N_4 achieves better resonant depth than the conventional configuration. The ER of the conventional biosensor without a Si_3N_4 is 2dB, and the proposed biosensor with a silicon nitride layer is 6.8dB.

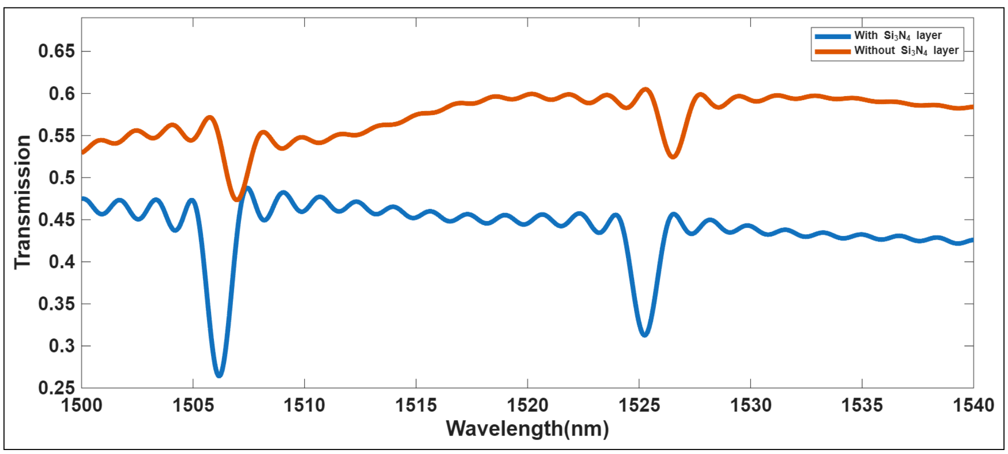

Fig. 8. Transmission Spectrum with and without Si_3N_4.

7.3. RRAMZI biosensor for measuring different concentrations of glucose

To measure glucose concentration, the analyte is applied to the ring resonator, which is coupled to the sensing arm of the biosensor. When glucose comes into contact with the cladding, it interacts with the evanescent field, resulting in a change in the redeffective refractive index(n_{eff}). This change is used to detect the concentration of glucose in the sample. The sensing process involves three main steps. First, the analyte is introduced. In this step, a sample containing glucose is applied to the sensor surface, which is coated with glucose oxidase. In the second step, a biochemical reaction occurs between the glucose and the enzyme. In the third step, this reaction causes a change in the n_{eff}, which corresponds to the glucose concentration. As the glucose concentration changes, the effective number of photons, n_{eff}, also changes. This causes a shift in the resonant peak of the transmission spectrum. Figure 10(a) shows the transmission spectrum for different concentrations of glucose, indicating non-diabetic, pre-diabetic, and diabetic levels. A glucose concentration below 100 mg/dl is considered non-diabetic. A level of around 120 mg/dL is considered pre-diabetic, and 150 mg/dL or higher is considered diabetic, as calculated by equation (20) and plotted in Fig. 9. Figure 10(b) show the variation of the n_{eff} and resonant wavelength with respect to different glucose concentrations [26].

$$n_c = 0.00011889.C_G.K + 1.33230545 \tag{20}$$

Where C= Concentration of Glucose, K= Concentration factor=1.

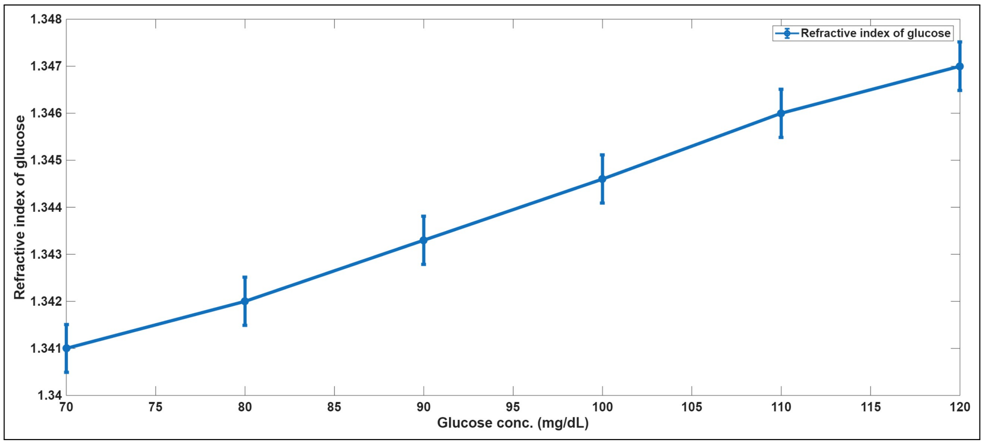

Fig. 9. Variation of the Refractive index with glucose conc. with tolerance band ±5%.

8. RAMZI with $FSiO_2$

In this section the considered FSiO $_2$ buffer, as it offers the advantage of enhanced sensitivity. The optimization of the Coupling gap and coupling length is the same as the previous section, but buffer thickness has to be optimized in this section, and then the sensitivity of the biosensor is measured.

8.1. Optimisation of buffer thickness

The buffer layer thickness must be optimized to achieve a good quality factor. The buffer thickness was optimized from 0.1μm to 0.25μm and then set to 0.2μm. The Fig. 11 shows the variation of the Transmission spectrum with buffer thickness.

8.2. Comparison with conventional biosensor with same dimensions

One main innovation of this biosensor is the addition of $FSiO_2$, which will enhance the evanescent field out of the core. Due to this, the penetration depth of the evanescent field increases, thereby enhancing sensitivity.The RRAMZI without buffer provide sensitivity of 370nm/RIU and with buffer provides a sensitivity of 400nm/RIU. The transmission spectrum is as shown in Fig. 12.

8.3. RAMZI as biosensor

In this section, the analyte is applied and measured, corresponding to the change in refractive index. The analyte used in this study is blood glucose. The transmission spectrum for different concentration of glucose is plotted in Fig. 13(a). The variation of resonating wavelength with respect to glucose concentration is as shown in Fig. 13(b).

Biomedical Optics EXPRESS

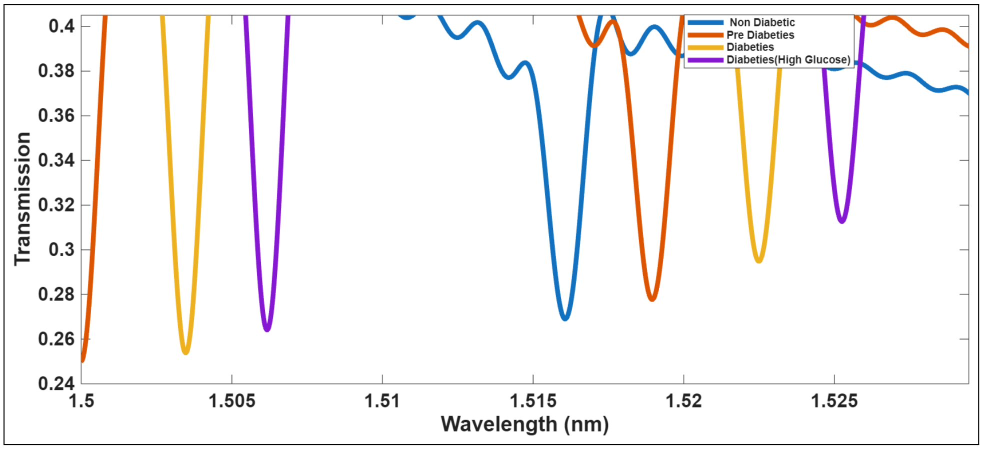

(a)

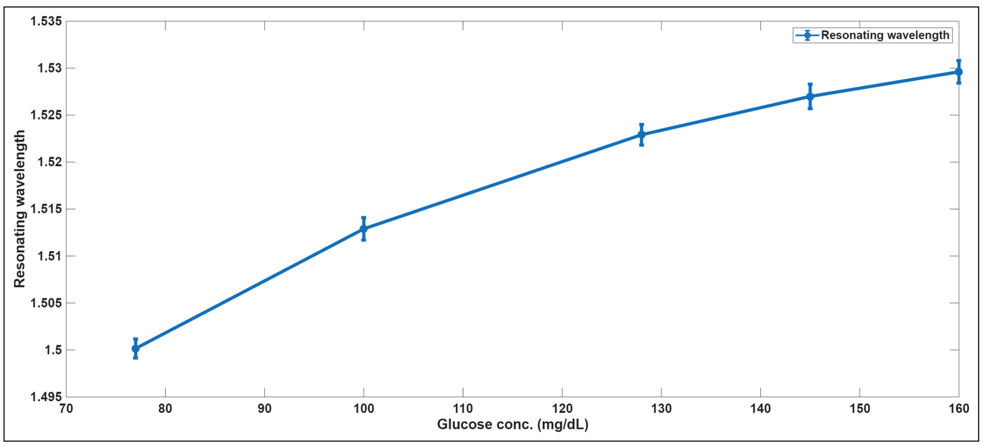

(b)

Fig. 10. Transmission Spectrum for (a) different concentration, (b) Resonating Wavelength, for different RI corresponding to concentration of glucose having tolerance band ±5%.

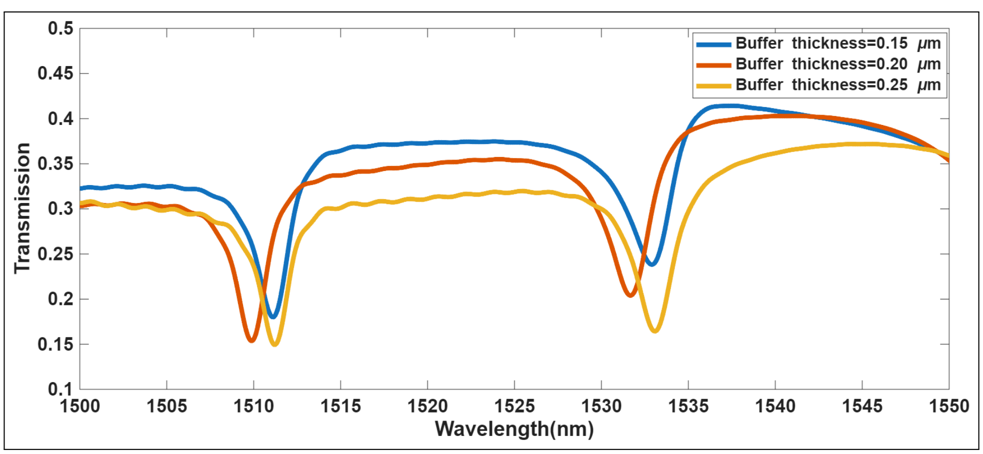

Fig. 11. Transmission spectrum.

Biomedical Optics EXPRESS

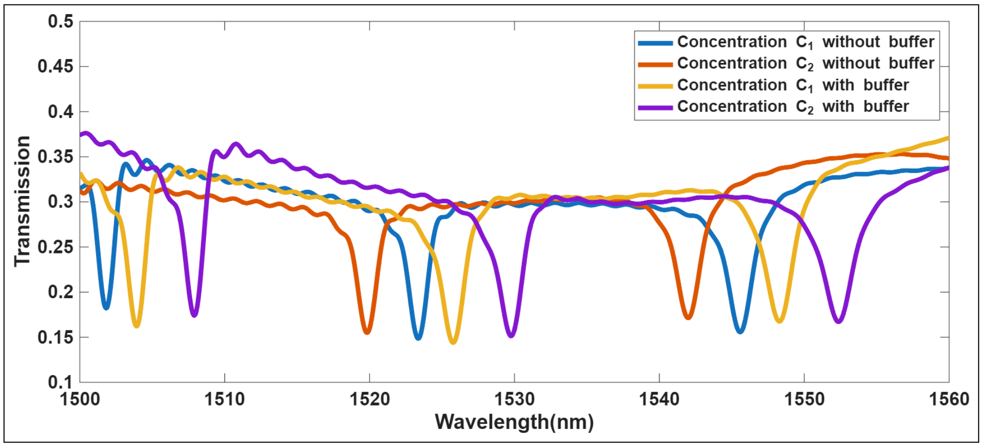

Fig. 12. Comparision of proposed biosensor with conventional biosensor.

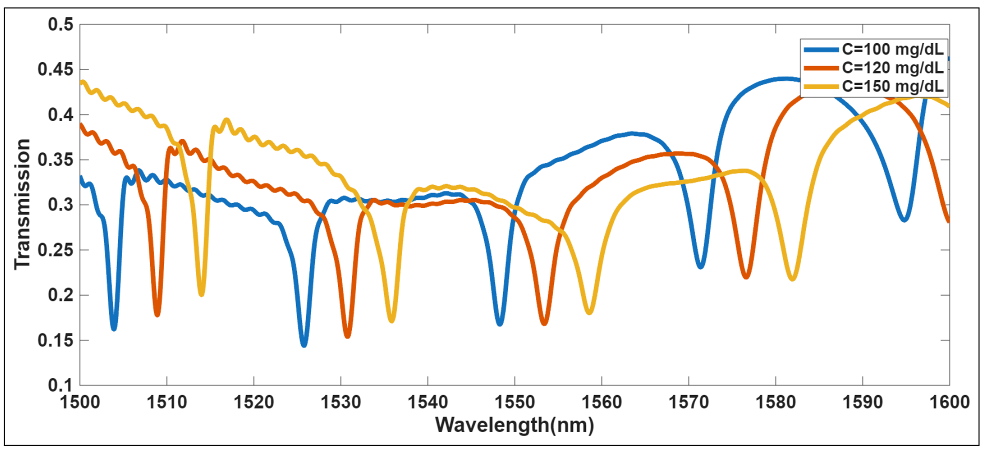

(a)

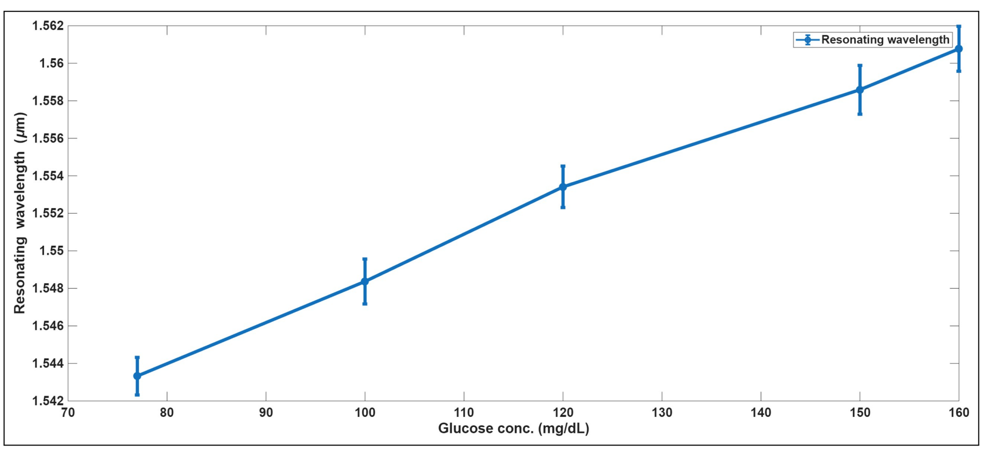

(b)

Fig. 13. (a) Transmission Spectrum for differnt concentration of analyte and (b) Resonating wavelength for different concentration of glucose having tolerance band ±5%.

8.4. Comparison for proposed biosensor with other biosensors

The biosensor performance is compared in terms of Sensitivity(S), FOM and Q in table 1. RR [23] is a basic integrated device designed with SiO_2 as substrate and Si core. It has a sensitivity of about 7 nm/RIU. This RR [25] is the modified version of RR with sensitivity 65 nm/RIU. The Micro Ring(MR) coupled MZI and RAMMZI [27]. of literature have a sensitivity of around 111 137.50 nm/RIU. So cascading is preferred than normal for enhancing sensitivity. This proposed RRAMZI with Si3N4 buffer provides a maximum sensitivity of 140 nm/RIU, with a Q of 1.43×10^3.Proposed RRAMZI with $FSiO_2$ provide the sensitivity of 400nm/RIU.

Table 1. Device Performance Comparison

Device	Sensitivity	Q	
WGM RR [23]	7	$1.131{\times}10^3$	
RR [24]	21	-	
RR [25]	65	$1.2{\times}10^3$-	
MR coupled MZI [26](EXP)	111	-	
RAMZI [27](Sim)	137.5	-	
This work	140	$1.435\text{x}10^3$	
This work	400	-	-

9. Conclusion

In this proposed two Racetrak Ring Assisted Mach-Zehnder Interferometer (RRAMZI) configuration with intermediate buffer layer is designed and analyzed. The novelty of structure is addition of buffer layer. Depending on buffer material it offered advantages of enhancement in resonant depth and penetration depth. If Silicon Nitride buffer used it enhances quality factor of biosensor by enhancing resonant depth. If Flourinated silicon dioxide buffer material used as buffer it enhances sensitivity. The transmission spectrum is plotted for two configurations and reported a quality factor of 1.435×10^3, and sensitivity of 400nm/RIU. The designing of RRAMZI biosensor is done by considering practical feasibility .

Acknowledgment. This work supported by CSIR.

Disclosures. Grammarly and Chat gpt used for grammar correction and rephrasing.

Data availability. All data generated or analysed during this study are included in this article.

References

1. A. Yariv, *Photonics*, Sixth edition (Oxford University press, 2007).
2. S. Samanta, P. Banerji, and P. Ganguly, "Effective index-based matrix method for silicon waveguides in SOI platform," Optik **126**(24), 5488–5495 (2015).
3. L. Enxiao, H. Shoman, D. M. Ratner, *et al.*, "Silicon Photonic Biosensors Using Label-Free Detection," Sensors **18**(10), 3519 (2018).
4. A. A. Kalam, Md. Jahirul Islam, and Md. Rejvi Kaysir., "Numerical analysis of Mach-Zehnder interferometer based optical sensors incorporating WGM ring resonator," *2020 11th International Conference on Electrical and Computer Engineering (ICECE).*, (IEEE).
5. M. Shwetha, M. Kumar, and K. Narayan, "Modeling and simulation of opto-fluidic based Mach-Zehnder interferometer for biosensing application," In *2015 Workshop on Recent Advances in Photonics (WRAP)* pp. 1–4 (IEEE, 2015).
6. Q. Liu, X. Tu, K. W. Kim, *et al.*, "Highly sensitive Mach-Zehnder interferometer biosensor based on silicon nitride slot waveguide," Sens. Actuators, B **188**, 681–688 (2013).
7. C. Tatevik, R. Guider, L. Pasquardini, *et al.*, "Asymmetric Mach–Zehnder interferometer based biosensors for aflatoxin M1 detection," Biosensors **6**(1), 1 (2016).
8. S. Yuze and X. Fan, "Optical ring resonators for biochemical and chemical sensing," Anal. Bioanal. Chem. **399**(1), 205–211 (2011).
9. L. Na, S. Wang, J. Lv, *et al.*, "Refractive index biosensor based on topological ring resonator," Opt. Commun. **541**, 129542 (2023).

Biomedical Optics EXPRESS

10. C. Xiaoyang, H. Jianxun, S. Andrew, *et al.*, "Fabrication of a high-Q factor ring resonator using LSCVD deposited Si3N4 film," Opt. Mater. Express **7**(7), 2182 (2017).
11. Y. Hong, H. Ge, and J. Hong, "Compact biosensors based on thin film silicon nitride microring resonators," J. Phys.: Conf. Ser. **2012**(1), 012037 (2021).
12. S. Alam, S. A. Chanu, U. Biswas, *et al.*, "Racetrack ring resonator based refractive index sensor for biosens- ing application," In *2025 IEEE Guwahati Subsection Conference (GCON)* (pp. 1–5) IEEE (2025).
13. F. Khozeymeh and M. Razaghi, "Optimized bent part coupling SiON race- track resonators for biological sensing," IEEE Sens. J. **19**(4), 1299–1306 (2019).
14. M. A. Butt, L. Kozlowski, M. Golas, *et al.*, "Numerical and experimental demonstration of a silicon nitride- based ring resonator structure for refractive index sensing," Appl. Sci. **14**(14), 6082 (2024).
15. Y. Chang, B. Dong, Y. Ma, *et al.*, "Vernier effect-basedtunable mid-infrared sensor using silicon-on-insulator cascaded rings," Opt. Express **28**(5), 6251–6260 (2020).
16. Y. Zhang, J. Zou, Z. Cao, *et al.*, "Temperature-insensitive waveguidesensor using a ring cascaded with a Mach-Zehnder interferometer," Opt. Lett. **44**(2), 299–302 (2019).
17. A. Melloni, R. Costa, G. Cusmai, *et al.*, "Waveguide index contrast: Implications for passive integrated optical components," *Proceedings of 2005 IEEE/LEOS Workshop on Fibres and Optical Passive Components, 2005*, (IEEE, 2005).
18. S. Darmawan, Y. M. Landobasa, and M. K. Chin, "Phase engineering for ring enhanced Mach-Zehnder interferometers," Opt. Express **13**(12), 4580–4588 (2005).
19. F. L. Hsiao and C. Lee, "Novel biosensor based on photonic crystal nano-ring resonator," Procedia Chem. **1**(1), 417–420 (2009).
20. M. F. Hassan, R. H. Sagor, M. R. Amin, *et al.*, "Point of care detection of blood electrolytes and glucose utilizing nano-dot enhanced plasmonic biosensor," IEEE Sens. J. **21**(16), 17749–17757 (2021).
21. K. Manchikalapati, "Four layer integrated optical biosensor," *SPIE Advanced Biophotonics Conference (SPIE ABC 2023)*, Vol. 13076, SPIE, (2024).
22. K. A. Nagoor, *Control Systems*, (RBA Publications, 1998).
23. A. K. Sarkaleh, B. V. Lahijani, H. Saberkari, *et al.*, "Optical ring resonators: a platform for biological sensing applications," J. Med. Signals Sens. **7**(3), 185–191 (2017).
24. A. L. Evans, *Ring Resonator Photonic Sensing Device* (University of Waterloo, 2015).
25. L. Ali, M. U. Mohammed, M. Khan, *et al.*, "high-quality optical ring resonator-based biosensor for Cancer detection," IEEE Sens. J. **20**(4), 1867–1875 (2020).
26. T. Zhang, B. Li, C. P. Ho, *et al.*, "High sensitive silicon optical index sensor based on Ring-assisted Mach-Zehnder interferometer," *2013 International Conference on Optical MEMS and Nanophotonics (OMN), Kanazawa, Japan*, (2013), pp. 129–130.
27. J. Wang and D. Dai, "Highly sensitive Si nanowire-based optical sensor using a Mach–Zehnder interferometer coupled microring," Opt. Lett. **35**(24), 4229–4231 (2010).